

# Optical and X-ray characteristics of a newly discovered narrow-line quasi-stellar object: RX J1334.2+3759

G. C. Dewangan,<sup>1\*</sup> K. P. Singh,<sup>1</sup> L. R. Jones,<sup>2</sup> I. M. McHardy,<sup>3</sup> K. O. Mason<sup>4</sup> and A. M. Newsam<sup>5</sup>

<sup>1</sup>Department of Astronomy & Astrophysics, Tata Institute of Fundamental Research, Mumbai, India 400 005

<sup>2</sup>School of Physics & Astronomy, University of Birmingham, Birmingham B15 2TT

<sup>3</sup>Astrophysics Research Institute, Liverpool John Moores University, Liverpool, CH41 1LD

<sup>4</sup>Mullard Space Science Laboratory, University College London, Holmbury St Mary, Dorking, Surrey RH5 6NT

<sup>5</sup>Department of Physics and Astronomy, University of Southampton, Highfield, Southampton SO17 1BJ

Accepted 2001 April 9. Received 2001 January 15; in original form 2000 August 2

## ABSTRACT

We report the discovery of a narrow-line quasi-stellar object (NLQSO) RX J1334.2+3759 with a steep soft X-ray spectrum. Soft X-ray emission from the NLQSO is highly variable. Changes in the intensity by a factor of  $\sim 2$  have been detected in the *ROSAT* Position Sensitive Proportional Counter (PSPC) observations of RX J1334.2+3759 on time-scales of  $\sim 20\,000$ – $40\,000$  s. Rapid variability events have also been observed from RX J1334.2+3759. The most extreme variable event has  $\Delta L/\Delta t = (1.95 \pm 1.02) \times 10^{42}$  erg s<sup>-2</sup> corresponding to a change in the intensity by a factor of  $\sim 4$  within  $\leq 400$  s. The PSPC spectra of the NLQSO can be well represented by a power law of photon index  $\Gamma_X \sim 3.8$ , modified by an absorbing column local to the source ( $\Delta N_H \sim 3.3 \times 10^{20}$  cm<sup>-2</sup>) over and above that caused by our own Galaxy ( $N_H = 7.9 \times 10^{19}$  cm<sup>-2</sup>). The intrinsic soft X-ray luminosity of RX J1334.2+3759 is estimated to be  $\sim 2.2 \times 10^{44}$  erg s<sup>-1</sup> in the energy band of 0.1–2.0 keV. The optical spectrum of RX J1334.2+3759 is typical of the narrow-line Seyfert 1 (NLS1) galaxies showing strong Balmer H $\beta$ , H $\alpha$ , and forbidden line of [O III] $\lambda$ 5007. Fe II multiplets, usually present in the optical spectra of NLS1 galaxies, are also detected from RX J1334.2+3759. Decomposition of the H $\beta$  and H $\alpha$  line profiles shows the presence of narrow [full width at half-maximum (FWHM)  $\sim 880$  km s<sup>-1</sup>] and broad (FWHM  $\sim 2850$  km s<sup>-1</sup>) components in the spectrum of RX J1334.2+3759. The narrow-line region of RX J1334.2+3759 appears to be significantly different from those of normal Seyfert galaxies. A possible explanation for the observed properties of the narrow-line region and the broad-line region is suggested in terms of density enhancements.

**Key words:** galaxies: active – galaxies: individual: RX J1334.2+3759 – galaxies: nuclei – X-rays: galaxies.

## 1 INTRODUCTION

Narrow-line Seyfert 1 (NLS1) galaxies are considered to be a special class of ‘normal’ Seyfert 1 galaxies because of their peculiar properties that distinguish them from the latter class. They are characterized by their optical spectra having permitted lines that are narrower than those in the normal Seyfert 1 galaxies, e.g. full width at half-maximum (FWHM) of H $\beta$  line is  $\leq 2000$  km s<sup>-1</sup>, relatively weak forbidden lines, ([O III] $\lambda$ 5007/H $\beta$ )  $< 3$  (Osterbrock & Pogge 1985; Goodrich 1989), and strong Fe II emission. X-ray observations with *Einstein* (e.g. Puchnarewicz et al. 1992) and *ROSAT* (e.g. Boller, Brandt & Fink 1996) have revealed that

NLS1 galaxies have distinctive soft X-ray properties as well. NLS1 galaxies show steep soft X-ray spectra with little or no absorption above the Galactic values along their respective lines of sight (Grupe et al. 1998). They often show rapid and large amplitudes as well as long-term X-ray variability (Boller et al. 1993; Brandt, Pounds & Fink 1995; Grupe et al. 1995a,b). In spite of the dominance of soft X-ray emission, the soft X-ray luminosities of the NLS1 galaxies are similar to those of normal Seyfert 1s. High-luminosity analogues of the NLS1 class, however, do exist. Prototypes of this class are – a narrow-line quasi-stellar object (or NLQSO) I Zw 1 (Phillips 1976), PHL 1092 (Brandt 1995; Forster & Halpern 1996; Lawrence et al. 1997), PKS 0558–504 (Remillard et al. 1991), and PG 1404+226 (Ulrich et al. 1999).

The spectral energy distribution (SED) from far-infrared (FIR)

\*E-mail: gulab@tifr.res.in

to X-rays of NLS1 galaxies appears to be similar to that of broad-line Seyfert 1 galaxies, but the UV luminosities of NLS1 galaxies tend to be smaller than those of Seyfert 1s (Rodríguez-Pascual, Mas-Hesse & Santos-Lleó 1997). The lower UV luminosity of NLS1 galaxies compared to normal Seyfert 1s could be because of the shift of the Big Blue Bump (BBB) towards higher energies. The steep soft X-ray spectrum could be the high energy tail of the BBB (Mathur 2000). To explain the relatively narrow width (FWHM  $\sim 2000 \text{ km s}^{-1}$ ) of the  $H\beta$  line in the NLS1 galaxies as compared to those (FWHM  $\sim 5000 \text{ km s}^{-1}$ ) in the Seyfert 1 galaxies, Wandel (1997) has argued that the steeper soft X-ray continuum has a higher ionizing power, resulting in an extended broad-line region (BLR), and hence a smaller velocity dispersion and narrower emission lines. Alternative views involve the virialized motion of a similar size BLR around a smaller black hole mass in NLS1s compared to those in Seyfert 1s (see Laor et al. 1997a; Brandt & Bolter 1998), and disc inclination effects (e.g. Osterbrock & Pogge 1985). The weakness of the forbidden line,  $[\text{O III}]\lambda 5007$ , relative to  $H\beta$  has not been understood. The importance of the decomposition of Balmer lines,  $H\alpha$  and  $H\beta$ , into narrow and broad components has been realized only recently in order to study the narrow-line region (NLR) and BLR emission line ratios in the NLS1 galaxies. Recent work of Rodríguez-Ardilla et al. (2000) has revealed that emission line ratios from the NLR of NLS1 are different from those observed in Seyfert galaxies, e.g.  $([\text{O III}]\lambda 5007/H\beta) = 0.8 - 5.0$  in the NLR of seven NLS1 galaxies, which is significantly different from the value  $\sim 10$  observed in the NLR of Seyfert galaxies. The reason for the observed difference has not been understood satisfactorily. Also, there are only a few NLS1 galaxies for which the NLR emission line ratios have been determined. Therefore, it is important to study the NLR and BLR emission line ratios in the other NLS1 galaxies.

In this paper, we present soft X-ray and optical emission line properties of a new NLQSO—RX J1334.2+3759, and investigate the origin of the NLR and BLR emission line ratios. The object, RX J1334.2+3759, was identified as an ultrasoft X-ray source by Singh et al. (1995) based on the White, Giommi & Angelini Catalogue (hereafter WGACAT: White, Giommi & Angelini 1994). Using deep *ROSAT* Position Sensitive Proportional Counter (PSPC) observations, the optical counterpart of the X-ray source RX J1334.2+3759 was identified by McHardy et al. (1998). The basic parameters of RX J1334.2+3759 are given in Table 1. The paper is structured as follows: in the next section, we describe the X-ray and optical spectroscopic observations followed by

**Table 1.** Basic parameters of RX J1334.2+3759.

Position<sup>1</sup>:  $\alpha(J2000) = 13^{\text{h}} 34^{\text{m}} 10^{\text{s}}.6$ ;  $\delta(J2000) = +37^{\circ} 59' 56''.0$   
 Redshift<sup>2</sup>:  $z = 0.3858 \pm 0.0004$ .  
 Magnitude<sup>1</sup>:  $R = 19.5$ .

<sup>1</sup> McHardy et al. (1998)

<sup>2</sup> Present paper

**Table 2.** Details of *ROSAT* observations of RX J1334.2+3759.

Serial no.	Sequence no.	Instrument	Offset (arcmin)	Start time Y, M, D, UT	End time Y, M, D, UT	Exposure time (s)	Count rate <sup>a</sup> $10^{-2} \text{ count s}^{-1}$
1.	RH900717N00	HRI	8.207	1997 06 04 16:12:58	1997 07 13 22:26:43	201513	$0.41 \pm 0.02$
2.	RP900626N00	PSPC	8.207	1993 06 19 22:24:46	1993 07 16 23:06:28	37658	$1.93 \pm 0.07$
3.	RP700283N00	PSPC	8.207	1991 06 23 20:59:40	1991 06 26 20:44:16	71803	$1.71 \pm 0.09$

<sup>a</sup> Mean count rates after background subtraction in the energy band of 0.1–2.4 keV.

analyses of the X-ray data and the optical spectrum in Section 3. We discuss our results in Section 4 followed by conclusions in Section 5.

Throughout the paper, luminosities are calculated assuming isotropic emission, a Hubble constant of  $H_0 = 75 \text{ km s}^{-1} \text{ Mpc}^{-1}$  and a deceleration parameter of  $q_0 = 0$  unless otherwise specified.

## 2 OBSERVATIONS

### 2.1 X-ray

The region of the sky containing the source RX J1334.2+3759 was observed twice with the *ROSAT* (Trümper 1983) PSPC during 1991–1993, and once with the High Resolution Imager (HRI) (Pfeffermann et al. 1987) in 1997 June 19–July 16. The two PSPC observations carried out during 1991 June 23–26, and 1993 June–July together comprise the second deepest *ROSAT* PSPC survey. These observations were targeted at  $\alpha(2000) = 13^{\text{h}} 34^{\text{m}} 37^{\text{s}}.0$ ,  $\delta(2000) = +37^{\circ} 54' 44''$  in the sky with an extremely low obscuration because of the matter in our Galaxy ( $N_{\text{H}} = 7.9 \times 10^{19} \text{ cm}^{-2}$ ). The PSPC deep survey data have already been reported by McHardy et al. (1998). The HRI observation was also a deep survey (exposure time = 201513 s) and was carried out in the same region of the sky as the PSPC deep surveys. The details of the *ROSAT* observations are given in Table 2. The off-sets of RX J1334.2+3759 from the field centres are also listed in Table 2. *ROSAT* X-ray data corresponding to the above observations were obtained from the public archives maintained at the High Energy Astrophysics Science Archive Research Center (HEASARC) in USA, and analysed by us using *PROS* and *FTOOLS*.

### 2.2 Optical

An optical spectrum of RX J1334.2+3759 was obtained on the night of 1994 April 7 with the Multi Object Spectrograph (MOS) on the 3.6-m Canada France Hawaii Telescope (CFHT) as a part of a program to identify X-ray sources (McHardy et al. 1998). A  $3001 \text{ mm}^{-1}$  grism in the first order with a Lorel3 Charge-coupled devices (CCD) detector was used to cover a wavelength range of 4000–9000 Å with  $\sim 15\text{-}\text{Å}$  resolution. The integration time was 2700 s. For details of the reduction see McHardy et al. (1998). The flux calibration is uncertain because the slitlets were not aligned at the parallactic angle.

The optical *R*-band image of RX J1334.2+3759 was obtained from the 2.5-m Isaac Newton Telescope (INT) using the wide-field camera on the night of 1999 April 19. The exposure time was 1200 s. The pixel scale is 0.333 arcsec per pixel. The seeing (FWHM) was  $\sim 1.3$  arcsec.

## 3 ANALYSIS AND RESULTS

The X-ray source, presented in this paper, was identified with

an optical object ( $R = 19.5$ ) by overlaying the contours of high-resolution (central FWHM of  $\sim 4$  arcsec) X-ray image obtained from *ROSAT* HRI observations on to the  $R$ -band optical image. HRI images were extracted and smoothed by convolving with a Gaussian of  $\sigma = 2$  arcsec using the *PROS* software package. X-ray contours overlaid on to the  $R$ -band optical image are shown in Fig. 1. Two fainter point objects about 4 and 10 arcsec away from RX J1334.2+3759 are seen on the overlay. The  $R$  magnitudes of these objects are  $\sim 22.3$  (nearest; hereafter object A) and  $\sim 22.9$  (object B) estimated from the  $R$ -band image and known  $R$  magnitude of RX J1334.2+3759. Object B is unlikely to be the optical counterpart of the X-ray source because of its distance from the X-ray peak. On the other hand, object A is unresolved and could contribute the X-ray intensity. In order to investigate the amount of X-ray emission from object A, we calculate the ratio of soft X-ray to  $R$ -band fluxes,  $f_X/f_R$ , for 22 QSOs including RX J1334.2+3759, which are within a circle of radius 15 arcmin

(Dewangan et al., in preparation). The flux ratios were calculated using the relation

$$\log\left(\frac{f_X}{f_R}\right) = \log(f_X) + \frac{m_R}{2.5} + 3.5 \quad (1)$$

where  $m_R$  is the  $R$ -band magnitude. The soft X-ray fluxes of all the QSOs have been derived from the *ROSAT* PSPC observation of 1991 listed in Table 2 (Dewangan et al., in preparation). The ratio,  $f_X/f_R$ , for the QSOs ranges from 0.003 to 0.040 with a mean value of  $0.014 \pm 0.010$ . If we assume object A to be the counterpart of the X-ray source, then the ratio ( $f_X/f_R$ ) is estimated to be  $\sim 0.20$  for A. A comparison of this ratio with that obtained for the QSOs shows that  $f_X/f_R$  for object A is much higher than that for the QSOs. However,  $f_X/f_R$  for RX J1334.2+3759 is 0.017 which is similar to that of other QSOs. If the object A is also similar to the QSOs, the contribution of this source to the total X-ray emission is expected to be  $\sim 7$  per cent.

The total source counts for RX J1334.2+3759 were obtained from the unsmoothed PSPC images using a circle of radius of 1.6 arcmin centred on the peak position, and after subtracting the background estimated from five nearby circular regions with their centres  $\sim 7.0$  arcmin away from the source. This was done using the *XSELECT* program in the *FTOOLS* (version 5.0) software package. The HRI count rate for RX J1334.2+3759 was extracted from a circle of radius 25 arcsec centred on the peak position, after subtracting the background estimated from an annulus of width 1.5 arcmin with the same centre and with an inner circle radius of 2 arcmin. The count rates thus estimated are given in Table 2.

### 3.1 X-ray light curves

In order to investigate the time variability of soft X-ray emission from RX J1334.2+3759, we have extracted the light curves from the *ROSAT* PSPC observations. The light curves for the source and the background were extracted using the ‘*XSELECT*’ package in the PSPC energy band of 0.1–2.4 keV containing all the X-ray photons falling within ‘good time intervals’. The time bin size is 500 s so that on an average each bin has  $\sim 10$  counts. The source regions and the background regions were the same as described above. It was found that the background was highly variable during the observation of 1993 June 19. Therefore, the light curve of RX J1334.2+3759 obtained from the 1993 observation is not suitable for variability studies. During the observation of 1991 June 23, the background was reasonably constant. A constant count rate fitted to the background light curve gives the best-fitting minimum value of  $\chi^2 = 73.54$  for 75 degrees of freedom. The background subtractions were carried out after appropriately scaling the background light curve to have the same area as the source extraction area. The background subtracted light curve of RX J1334.2+3759 and the background light curve are shown in Fig. 2. A remarkable variability in the soft X-ray flux from RX J1334.2+3759 can be seen in Fig. 2. A constant count rate fit to the light curve of RX J1334.2+3759 gives the minimum value of  $\chi^2$  as 154.6 for 75 degrees of freedom. X-ray emission from RX J1334.2+3759 changed by a factor of  $\sim 2$  on time-scales of 20000–40000 s. Variability on shorter time-scales is also observed on several occasions notably at the beginning of the observation, after  $\sim 200\,000$  s, and after  $\sim 240\,000$  s. The most significant and extreme variable event is that observed around 200 000 s which is shown in Fig. 3 with a smaller bin size of 200 s. The nine data points to the left of the variability event (only two data points are shown in Fig. 3) have a mean value of  $(2.21 \pm 1.26) \times 10^{-2}$  counts  $s^{-1}$ . We treat this

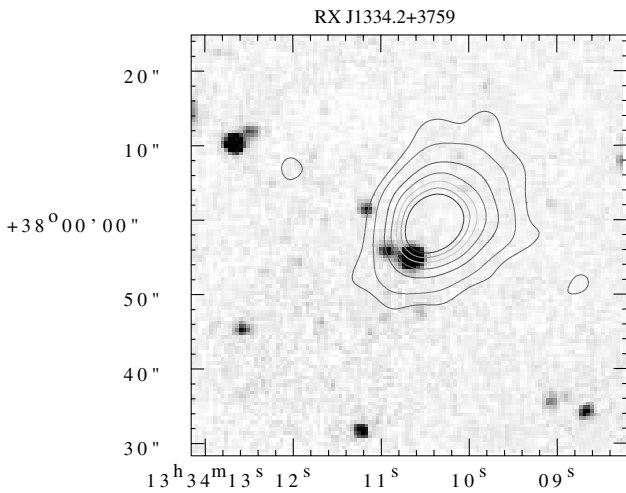


**Figure 1.** Contours of the *ROSAT* HRI intensity of RX J1334.2+3759 overlaid on the  $R$ -band optical image. For clarity, only the contours at 6, 10, 20, 30, 40, 50 and 60 per cent of the peak intensity are shown. The X-ray contours have been generated from the HRI image after smoothing by a Gaussian of  $\sigma = 2$  arcsec. The HRI image was created from the data observed on 1997 July 7 (exposure time = 201513 s).

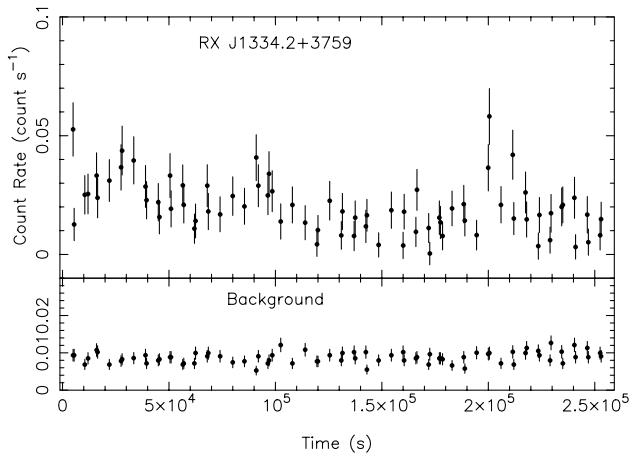


**Figure 2.** Background subtracted *ROSAT* PSPC light curve of RX J1334.2+3759 observed on 1991 June 23 and the simultaneously obtained background light curve (solid line). The bin size in the light curve is 500 s. The start time of the observation was 1991 June 23 20:59:40 UT.

average count rate as the rate in the quiescent state from which the flare arises. After 200 200 s since the beginning of the observation, the PSPC count rate began to increase reaching a maximum of  $(8.90 \pm 2.25) \times 10^{-2} \text{ count s}^{-1}$  at 200 600 s. Thus, an increase in the count rate by a factor of  $\sim 4$  in  $\leq 400 \pm 141 \text{ s}$  ( $\leq 380 \pm 134 \text{ s}$  in the rest frame) is detected. Thus, for the variability event shown in Fig. 3, we find a change in the PSPC count rate of  $(6.69 \pm 2.58) \times 10^{-2} \text{ count s}^{-1}$ . This corresponds to a change in the intrinsic luminosity of  $(7.43 \pm 2.86) \times 10^{44} \text{ erg s}^{-1}$ , in the energy band of 0.1–2.0 keV, in the rest frame time interval of  $< 380 \pm 134 \text{ s}$ .

In order to investigate the long-term (time-scale of a few years) variation in the X-ray intensity of RX J1334.2+3759, we have converted the HRI count rate, obtained from the observation of 1997 June 4, into an equivalent PSPC count rate using the best-fitting model parameters ( $N_{\text{H}} = 3.3 \times 10^{20} \text{ cm}^{-2}$ ,  $\Gamma_{\text{X}} = 3.8$ ) obtained from the joint fit to the PSPC spectra (see Section 3.2). The equivalent PSPC count rate is estimated to be  $(2.22 \pm 0.11) \times 10^{-2} \text{ count s}^{-1}$ , which is similar to the PSPC count rates obtained during the observations of 1991 and 1993.

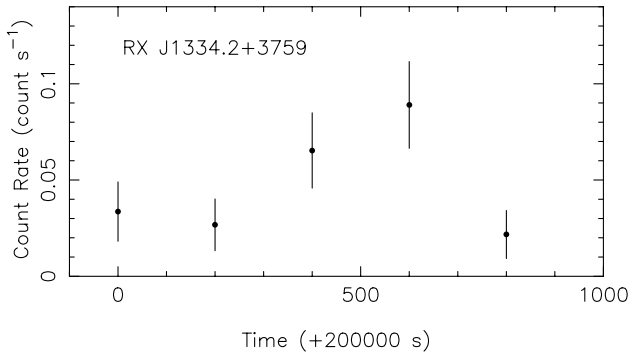


**Figure 3.** The most extreme variability event observed from RX J1334.2+3759 about  $2 \times 10^5 \text{ s}$  since the beginning of the observation on 1991 June 23. The bin size in the light curve is 200 s. The light curve is background subtracted. The start time of the observation was 1991 June 23 20:59:40 UT.

### 3.2 X-ray spectral analysis

Photon energy spectra of RX J1334.2+3759 were accumulated from their PSPC observations shown in Table 2. The same regions for the source and the background, as stated above, were used. The *ROSAT* PSPC pulse height data obtained in 256 pulse height channels were appropriately re-grouped to improve the statistics. X-ray spectra of RX J1334.2+3759 from the two observations thus obtained are shown in Fig. 4.

We used the XSPEC (Version 11.0) spectral analysis package to fit the data with spectral models. This requires a knowledge of the response of the telescope and the detector. An appropriate response matrix, provided by the *ROSAT* Guest Observer Facility at the High Energy Astrophysics Science Archive Research Center (HEASARC), was used to define the energy response of the PSPC. The off-axis calibration of the telescope has been appropriately taken into

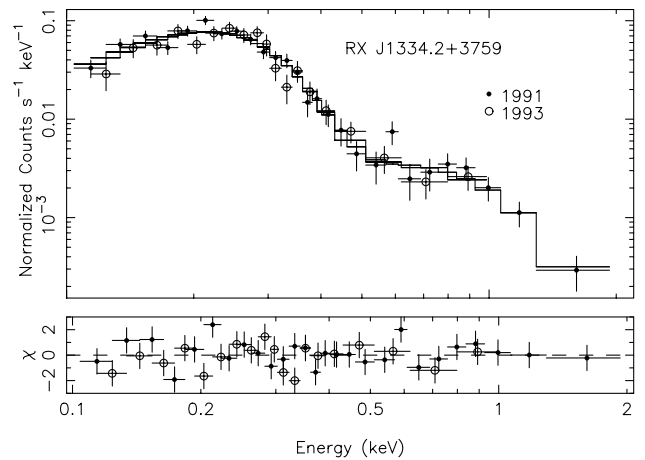


**Figure 4.** Spectral data from two observations and a model (histogram) fitted simultaneously to the *ROSAT* PSPC X-ray spectra of RX J1334.2+3759. The fitted model is a redshifted power law modified by absorbing columns present in our own Galaxy as well as in RX J1334.2+3759.

**Table 3.** Best-fitting model spectral parameters for RX J1334.2+3759.

Data	Model <sup>a</sup>	$N_{\text{H}}$ ( $10^{19} \text{ cm}^{-2}$ )	$\Delta N_{\text{H}}^b$ ( $10^{20} \text{ cm}^{-2}$ )	$\Gamma_{\text{X}}$ or $kT$ (eV)	$f_{\text{X}}^c$	$L_{\text{X}}^d$	$\chi^2/\nu^e$
1991 (June 23–July 26)	pl+abs <sub>Gal</sub>	$18.1^{+6.0}_{-4.7}$	–	$3.6^{+0.3}_{-0.3}$	8.8	1.71	0.97/24
	pl+abs <sub>Gal</sub>	7.9 (fixed)	–	$3.1^{+0.1}_{-0.1}$	8.22	0.72	1.58/25
	pl+abs <sub>Gal</sub> +abs <sub>source</sub>	7.9 (fixed)	$2.8^{+1.7}_{-0.8}$	$3.7^{+0.4}_{-0.3}$	8.8	1.9	0.96/24
1993 (June 19–July 16)	pl+abs <sub>Gal</sub>	$25.5^{+15.0}_{-9.9}$	–	$4.0^{+0.8}_{-0.6}$	8.55	2.94	0.960/16
	pl+abs <sub>Gal</sub>	7.9 (fixed)	–	$2.9^{+0.2}_{-0.2}$	8.3	0.68	1.64/17
	pl+abs <sub>Gal</sub> +abs <sub>source</sub>	7.9 (fixed)	$4.9^{+4.2}_{-2.8}$	$4.2^{+1.0}_{-0.7}$	8.6	3.66	0.96/16
1991 and 1993 <sup>f</sup>	pl+abs <sub>Gal</sub>	$19.8^{+5.4}_{-4.4}$	–	$3.7^{+0.3}_{-0.3}$	8.7	1.90	0.95/43
	pl+abs <sub>Gal</sub>	7.9 (fixed)	–	$3.0^{+0.1}_{-0.1}$	8.20	0.33	1.57/44
	pl+abs <sub>Gal</sub> +abs <sub>source</sub>	7.9 (fixed)	$3.3^{+1.5}_{-1.3}$	$3.8^{+0.3}_{-0.3}$	8.7	2.18	0.95/43
	abs+blackbody	7.9 (fixed)	–	135	9.73	0.4	1.74/44

<sup>a</sup>pl is the redshifted simple power-law model while abs<sub>Gal</sub>(abs<sub>source</sub>) is the photoelectric absorption model at  $z = 0$  ( $z = 0.3858$ ) using the Balucinska-Church & McCammon (1992) cross-sections. blackbody is the redshifted blackbody model.

<sup>b</sup>Excess  $N_{\text{H}}$  over the Galactic value.

<sup>c</sup>Observed flux in units of  $10^{-14} \text{ erg cm}^{-2} \text{ s}^{-1}$  in the energy band of 0.1–2.0 keV.

<sup>d</sup>Intrinsic soft X-ray luminosity in units of  $10^{44} \text{ erg s}^{-1}$  in the energy band of 0.1–2.0 keV.

<sup>e</sup>Minimum reduced  $\chi^2$  for  $\nu$  degrees of freedom.

<sup>f</sup>Data are jointly fit to the same spectral models.

account by creating and using an auxiliary response. The *ROSAT* PSPC spectra of RX J1334.2+3759, shown in Fig. 4, were used for fitting spectral models. The spectra from the two observations were first fitted separately with the redshifted power-law model with photon index,  $\Gamma_X$ , and absorption owing to an intervening medium with the absorption cross-sections as given by Balucinska-Church & McCammon (1992), and using the method of  $\chi^2$  minimization. The results of these fittings and the best-fitting model parameters are shown in Table 3. The errors quoted, here and below, were calculated at the 90 per cent confidence level based on  $\chi^2_{\min} + 2.71$ . As can be seen in Table 3, the best-fitting model parameters derived from the two observations are similar within errors. In order to better constrain the model parameters, we have jointly fitted spectral models to the two observed spectra and below, we discuss the joint model fitting in detail. The results of this fitting and the best-fitting spectral model parameters are listed in Table 3. The simple model, (power law + absorption at  $z = 0$ ), with  $\Gamma_X$  in the range of 3.4–4.0 and  $N_H$  in the range of  $1.5 \times 10^{20}$ – $2.5 \times 10^{20} \text{ cm}^{-2}$  is a good fit to both the spectra, as shown by the minimum reduced  $\chi^2$  ( $\chi^2_{\nu}$ ) value of 0.95 for 43 degrees of freedom. The absorbing column density thus derived by fitting the power-law model is in excess of the Galactic value ( $N_H = 7.9 \times 10^{19} \text{ cm}^{-2}$ ) measured from the 21-cm radio observations along the line of sight to the source (Dickey & Lockman 1990). This indicates that all the X-ray absorption may not be only because of matter in our own Galaxy but also because of matter local to the source. We next fixed the absorbing column to the Galactic value and fitted the power-law model to both spectra. There is an increase in the  $\chi^2_{\nu}$  value and the fit becomes worse ( $\chi^2_{\nu} = 1.57$  for 44 degrees of freedom) indicating that an additional component is needed. In order to determine the absorbing column local to the source, we introduced an additional absorbing column at the source redshift ( $z = 0.3858$ ) and carried out the power-law fitting. The best-fitting spectral parameters are again given in Table 3. The intrinsic absorption column density

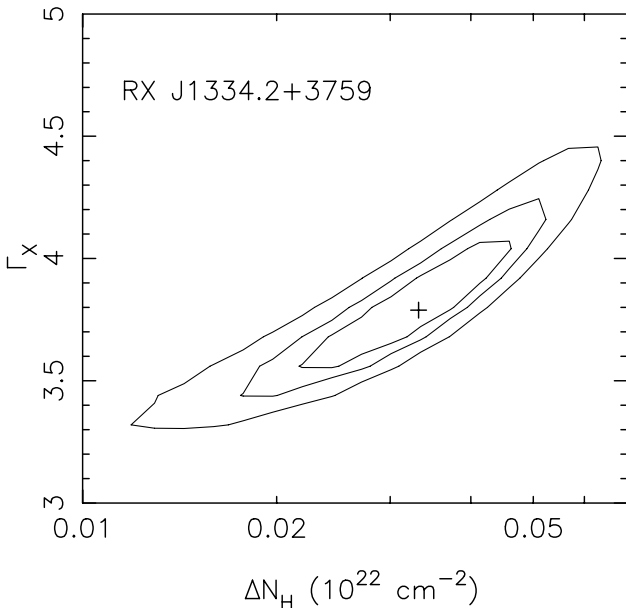


**Figure 5.** Allowed ranges of power law photon index and ‘excess’  $N_H$  ( $\Delta N_H$ ) (at  $z = 0.38$ ) for 68, 90 and 98 per cent confidence based on counting statistics derived from the joint-fit of the two PSPC spectra for RX J1334.2+3759. The ‘+’ marks the best-fitting value.

( $\Delta N_H$ ) thus derived is indeed small ( $3.3^{+1.5}_{-1.3} \times 10^{20} \text{ cm}^{-2}$ ). The best-fitting photon index is  $3.8^{+0.3}_{-0.3}$ .

Based on the  $\chi^2_{\nu}$  values, it is clear that a redshifted power-law model with Galactic plus intrinsic  $N_H$  is preferred over the model with  $\Delta N_H = 0$ . The power-law model absorbed by the Galactic and the intrinsic column is a significant improvement over the power-law model absorbed by the Galactic column alone, at 99.99 per cent confidence level based on an F-test (F-statistics value = 29.7 and probability =  $2.28 \times 10^{-6}$ ). Allowed ranges of  $\Gamma_X$  and  $\Delta N_H$  are shown in Fig. 5. The observed X-ray flux from the source RX J1334.2+3759 is estimated to be  $8.7 \times 10^{-14} \text{ erg cm}^{-2} \text{ s}^{-1}$  in the energy band of 0.1–2.0 keV. The intrinsic flux, estimated by setting  $N_H$  equal to zero, is found to be  $5.4 \times 10^{-13} \text{ erg cm}^{-2} \text{ s}^{-1}$  in the energy band of 0.1–2.0 keV. The intrinsic X-ray luminosity in the energy band of 0.1–2.0 keV is calculated to be  $2.2 \times 10^{44} \text{ erg s}^{-1}$ . We have also fitted the redshifted blackbody models absorbed by an intervening medium. The absorbing column density was fixed to the Galactic value as otherwise unphysically low values of  $N_H$ , lower than the Galactic  $N_H$ , are obtained. The best-fitting model parameters are given in Table 3. It is clear from the  $\chi^2_{\nu}$  that the PSPC spectra are not well represented by a simple blackbody model. However, a temperature of  $\sim 135 \text{ eV}$  is inferred for the blackbody.

### 3.3 Optical spectrum

The optical spectrum of RX J1334.2+3759 is shown in Fig. 6. The signal-to-noise ratio of the spectrum is  $\sim 13$ , as measured from the dispersion in the continuum region 6050–6150 Å in the spectrum. Strong emission lines of Balmer  $H\alpha$ ,  $H\beta$ , and the forbidden line [O III]  $\lambda 5007$  are readily observed. To measure the redshift of RX J1334.2+3759, we fitted Gaussians to the upper half of the  $H\alpha$ ,  $H\beta$ , and [O III]  $\lambda 5007$  line profiles. Using the fitted positions and the rest wavelengths of these lines, the redshift of RX J1334.2+3759 is derived to be  $0.3858 \pm 0.0004$ . The redshift quoted here is the average value derived from the above three lines and the error is the dispersion. The spectrum, shown in Fig. 6, is corrected to the rest wavelengths. Apart from the emission lines mentioned above, we have also identified several other emission lines such as [Ne V]  $\lambda 3426$ , [O II]  $\lambda 3727$ , [Ne III]  $\lambda 3869$ , He I  $\lambda 3969$ , H  $\gamma$   $\lambda 4340$ ,  $H\beta$ , Fe II  $\lambda 4924$ , and He I  $\lambda 5876$ . Also present in the spectrum is the Fe II emission seen as two broad humps at 4450–4700 Å and 5150–5350 Å. All the above lines have been marked in Fig. 6.

The Fe II blends complicate the measurement of the line strengths of  $H\beta$ , [O III]  $\lambda 5007$  etc. as a result of their contamination. In order to estimate their strength reliably and to measure the line fluxes, we have adopted the method of Boroson & Green (1992) and used their Fe II template. In order to use the Fe II template, we first ensured that the template and the spectrum of RX J1334.2+3759 are correctly redshifted and refer to the rest wavelengths. The template was then broadened to the FWHM of the  $H\beta$  line in the spectrum of RX J1334.2+3759 by convolving with a Gaussian of  $\sigma = 7.5 \text{ Å}$ . The smoothed Fe II template was scaled appropriately to match the intensity of the observed Fe II and then subtracted from the spectrum of RX J1334.2+3759. The procedure of Fe II subtraction is depicted in Fig. 7. Note that the Fe II subtracted spectrum has been shifted downwards for clarity. As a result of the Fe II subtraction, the continuum around the  $H\beta$  line has flattened implying that the Fe II model fits the observed Fe II well in the spectrum of RX J1334.2+3759. The rest frame equivalent width of Fe II was determined from the flux in the scaled

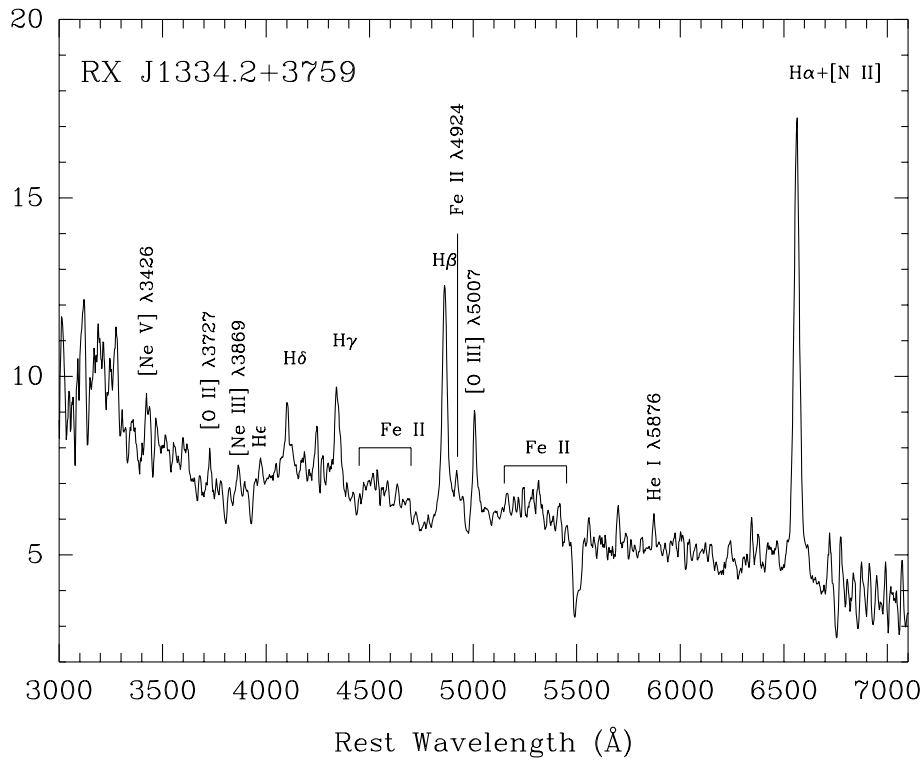


**Figure 6.** Optical spectrum of RX J1334.2+3759. The vertical scale represents the relative flux. The spectrum has been smoothed by a box filter of width 12.5 Å. The absorption feature at 5500 Å is because of atmospheric absorption.

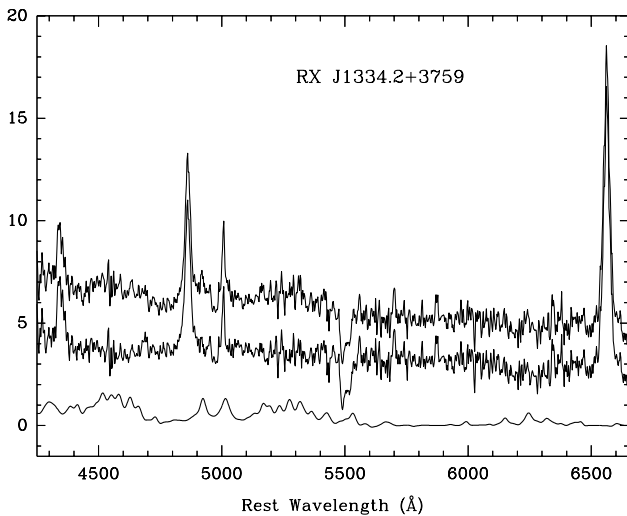


**Figure 7.** Subtraction of the Fe II template from the observed spectrum of RX J1334.2+3759. The vertical scale represents the relative flux. The top spectrum is the redshifted observed spectrum while the bottom one is the Fe II model for RX J1334.2+3759. The middle spectrum is the Fe II subtracted spectrum of RX J1334.2+3759. Note that the Fe II corrected spectrum has been shifted downward for visibility.

Fe II template between the rest wavelengths 4250 and 5880 Å, and the continuum flux density at 5050 Å in the Fe II subtracted spectrum. The equivalent width of Fe II is listed in Table 4.

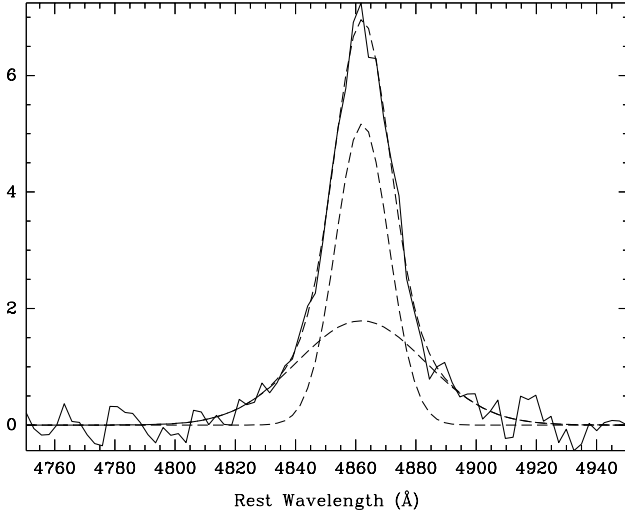
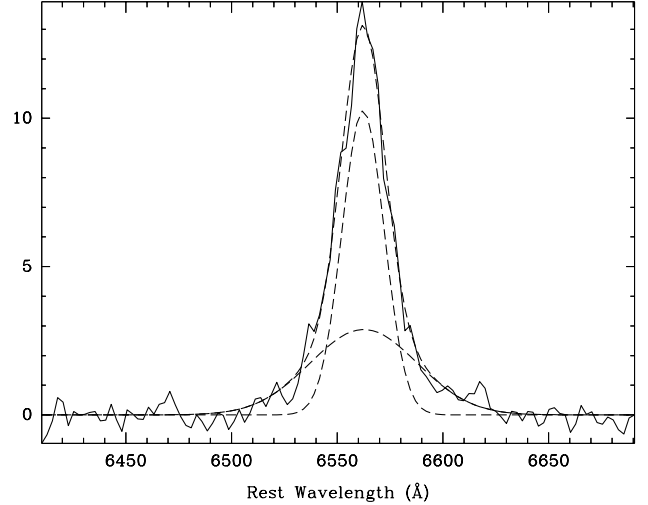
In order to measure the parameters of strong lines other than Fe II, we have used the continuum subtracted and Fe II corrected spectrum of RX J1334.2+3759. The continuum from the Fe II subtracted spectrum was removed by fitting a low-order

polynomial after excluding the emission lines. We have assumed that the emission lines can be represented by a single or a combination of Gaussian profiles. As a first step, we fitted a single Gaussian profile to the H $\beta$  line. The FWHM velocity of the best-fitting Gaussian is 1557 km s<sup>-1</sup>. It was, however, found that the broad wings and the peak of the H $\beta$  line are not well fitted by a single Gaussian profile. It was necessary, therefore, to introduce an additional component in order to represent the observed profile adequately. We then fitted two Gaussian profiles simultaneously to the H $\beta$  line. The decomposition of the H $\beta$  line into two Gaussians is shown in Fig. 8. The positions of the Gaussians were fixed at the rest wavelength of the H $\beta$  line while the amplitudes and the FWHMs were varied to achieve the best fit. The residuals from the best-fitted profile were found to be similar to the noise level near H $\beta$ . Thus we find that two Gaussians, a narrow component (FWHM  $\sim$  877 km s<sup>-1</sup>) and a broad component (FWHM  $\sim$  2853 km s<sup>-1</sup>) describe the observed H $\beta$  profile much better than a single Gaussian profile. The parameters of the H $\beta$  line obtained from the best-fitting profile are listed in Table 4. The equivalent widths, given in Table 4, refer to the continuum flux density, obtained from continuum fitting, at the rest wavelength of H $\beta$ . The [O III] $\lambda$ 5007 line has not been resolved. Its width is found to be comparable to the instrumental resolution. The strength of the [O III] $\lambda$ 5007 line was determined by integrating the line profile.

As a result of the poor instrumental resolution (FWHM  $\sim$  15 Å), it was not possible to decompose H $\alpha$  and [N II] $\lambda$ 6548,6583 lines. To measure reliably the FWHM and the equivalent width of H $\alpha$ , it is necessary to correct for the contribution of [N II] $\lambda$ 6548,6583. For this purpose, we have created templates for the [N II] $\lambda$ 6548,6583 lines from the [O III] $\lambda$ 5007 line. These lines are expected to have similar widths and are unresolved in the spectrum of RX J1334.2+3759. First, we isolated the [O III] $\lambda$ 5007

**Table 4.** Optical emission line parameters of RX J1334.2+3759.

Emission line	Broad Component		Narrow Component	
	FWHM ( $\text{km s}^{-1}$ )	Equivalent width ( $\text{\AA}$ )	FWHM ( $\text{km s}^{-1}$ )	Equivalent width ( $\text{\AA}$ )
H $\beta$	$2853 \pm 520$	$15.8 \pm 3.6$	$877 \pm 91$	$19.5 \pm 3.8$
[O III] $\lambda$ 5007	–	–	–	$5.0 \pm 0.5$
H $\alpha$	$2843 \pm 479$	$33.8 \pm 7.5$	$883 \pm 41$	54.5
Fe II	–	159	–	–

**Figure 8.** Decomposition of the observed H $\beta$  profile into two Gaussian components. The vertical scale represents the relative flux.**Figure 9.** Decomposition of the H $\alpha$  profile into two Gaussian profiles. The vertical scale represents the relative flux.

line in the wavelength region 4992–5018  $\text{\AA}$  from the continuum subtracted and the Fe II corrected spectrum of RX J1334.2+3759. The [O III] $\lambda$ 5007 line was then shifted to the rest wavelength of [N II] $\lambda$ 6583. To get the template for [N II] $\lambda$ 6583, the shifted [O III] $\lambda$ 5007 line was scaled to have flux that was 35 per cent of the actual flux of the [O III] $\lambda$ 5007 line, since the contribution of [N II] $\lambda$ 6583 to H $\alpha$  is  $\sim 35$  per cent of the flux of [O III] $\lambda$ 5007 (Ferland & Osterbrock 1986). We did not change the FWHM of [N II] $\lambda$ 6583 template from that of [O III] $\lambda$ 5007. To make the template for the [N II] $\lambda$ 6548 line, the [N II] $\lambda$ 6583 template was shifted to the rest wavelength of [N II] $\lambda$ 6548 and then scaled so that the ratio of fluxes of [N II] $\lambda$ 6583 and [N II] $\lambda$ 6548 is the same as the theoretical ratio of 2.96. To correct for the contribution of [N II] $\lambda$ 6548, 6583 to the H $\alpha$  line, the two templates, created above, were subtracted from the continuum subtracted and Fe II corrected spectrum of RX J1334.2+3759. This subtraction has little effect on the H $\alpha$  profile because the intensities of [N II] $\lambda$ 6548, 6583 lines are much smaller than that of H $\alpha$ . This is expected since the flux ratio,  $([\text{O III}]\lambda 5007/\text{H}\beta)$ , is very small ( $\sim 0.14$ ) for RX J1334.2+3759 which gives the flux ratio,  $([\text{N II}]\lambda 6548, 6583)/\text{H}\alpha \approx 0.016$  assuming the case B value of the flux ratio  $\text{H}\alpha/\text{H}\beta \sim 3.1$  (e.g. Osterbrock 1989). The H $\alpha$  profile is again poorly fitted by a single Gaussian. Applying the same decomposition technique, as was done for the H $\beta$  profile, we find that the profile of H $\alpha$  is best fitted by two Gaussians, one with a narrow component (FWHM  $\sim 883 \text{ km s}^{-1}$ ) and the other with a broad component (FWHM  $\sim 2843 \text{ km s}^{-1}$ ). The two-component profile fit to the H $\alpha$  is shown in Fig. 9. The equivalent widths, listed in Table 4, refer to the flux density at the rest wavelength of H $\alpha$  in the Fe II corrected spectrum.

## 4 DISCUSSION

RX J1334.2+3759 is luminous in optical and soft X-rays. Its optical luminosity ( $M_R \approx -22.7$  assuming  $H_0 = 50 \text{ km s}^{-1} \text{ Mpc}^{-1}$ ) and soft X-ray luminosity ( $L_X \approx 2.8 \times 10^{44} \text{ erg s}^{-1}$  in the energy band of 0.1–2.0 keV) are similar to that of a low-luminosity QSO. The object has been classified as a QSO by McHardy et al. (1998). Based on optical spectroscopy and analysis of publicly available X-ray data from *ROSAT* observations, we find that the newly discovered QSO RX J1334.2+3759 belongs to the NLS1 class. Therefore, it is referred to as NLQSO here. Its X-ray and optical characteristics are further discussed below.

### 4.1 Soft X-ray variability

Soft X-ray emission from RX J1334.9+3759 is highly variable (see Figs 2 and 3). During the 1991 observations, RX J1334.9+3759 showed soft X-ray variability on times-scales of  $\sim 20000$ – $40000$  s by a factor of  $\sim 2$ . Rapid variability events have also been detected from RX J1334.9+3759. The most significant and extreme variable event, shown in Fig. 3, has  $\Delta L/\Delta t > (1.95 \pm 1.02) \times 10^{42} \text{ erg s}^{-2}$ , which is similar to that of the extreme variable event observed from PHL 1092 (Brandt et al. 1999). Straightforward application of the efficiency ( $\eta$ ) limit:  $\eta > 4.8 \times 10^{-43} \Delta L/\Delta t$  (Fabian & Rees 1979), results in an extremely high efficiency ( $\eta > 0.93 \pm 0.49$ ). This can be compared with  $\eta \sim 0.3$  for an optimally accreting Kerr BH rotating at the maximum plausible rate (Thorne 1974). Thus the radiative efficiency for the extreme variable event shown in Fig. 3 appears to be substantially larger, and suggests relativistic effects

responsible for the extreme variable event. The suggestion that relativistic effects may be responsible for the extreme variability event can also be inferred as follows. The variability time-scale, in the absence of relativistic effects, provides an upper limit to the size of the X-ray emitting region,  $R < c\Delta t$ . For RX J1334.2+3759,  $R < 1.14 \times 10^{13}$  cm. SEDs of a sample of NLS1 galaxies (Rodríguez-Pascual et al. 1997) show that the soft X-ray luminosity of NLS1s can, at most, be 9 per cent of the bolometric luminosity. If we assume that the SED of RX J1334.2+3759 is similar to that of the other NLS1s, then the bolometric luminosity of RX J1334.2+3759 is expected to be  $\geq 2.4 \times 10^{45}$  erg s<sup>-1</sup>. If this luminosity is within the Eddington limit, then RX J1334.2+3759 must have a central mass,  $M > 2 \times 10^7 M_{\odot}$ . In that case, the radius of the last stable orbit,  $3R_s > 1.8 \times 10^{13}$  cm, would then be larger than the size of the X-ray emitting region, so photons should not escape.

Extremely rapid X-ray variability has also been observed in three other NLS1 class objects: PKS 0558–504 ( $\eta > 1.5$ ; Remillard et al. 1991), IRAS 13224–3809 ( $\eta > 0.09$ ; Boller et al. 1997), and PHL 1092 ( $\eta > 0.6$ ; Brandt et al. 1999) and relativistic effects have been suggested to be responsible for the enhanced X-ray variability.

#### 4.2 Soft X-ray spectral characteristics

The soft X-ray spectrum of RX J1334.2+3759 is very steep and is well represented by a power law of photon index,  $\Gamma_X = 3.8^{+0.3}_{-0.3}$  with an excess absorption,  $\Delta N_H \sim 3.3 \times 10^{20}$  cm<sup>-2</sup>, local to the source and apart from the Galactic absorption,  $N_H \sim 7.9 \times 10^{19}$  cm<sup>-2</sup> (see Table 3). Thus the soft X-ray spectrum of RX J1334.2+3759 is steeper than those of normal Seyfert 1s [ $\Gamma_X$  (90 per cent range) = 2.0–2.7], and similar to those of NLS1 galaxies [ $\Gamma_X$  (90 per cent range) = 2.3–3.7] (Grupe et al. 1998). The intrinsic absorption, inferred from the power-law model fit to the spectra of RX J1334.2+3759, is not high and is similar to those found in normal Seyfert 1s and NLS1 galaxies. The steeper power-law index and blackbody model fit to the PSPC spectra of RX J1334.2+3759 indicate the ultrasoft nature of this object. The derived temperature of the blackbody,  $kT \sim 135$  eV, is similar to those found in NLS1 galaxies (Brandt & Boller 1998). That this object is similar to the NLS1 galaxies in its nature, is further supported by the optical spectroscopic properties of RX J1334.2+3759 (see below). The excess soft X-ray emission of NLS1 galaxies is usually attributed to a higher accretion rate compared to the Eddington accretion rate ( $\dot{m} = \dot{M}/\dot{M}_{\text{Edd}}$ ) (Pounds, Done & Osborne 1995; Brandt & Boller 1998). The bolometric luminosity of RX J1334.2+3759,  $L_{\text{bol}} \geq 2.4 \times 10^{45}$  erg s<sup>-1</sup>, is about a factor of  $\sim 2$  higher than the Eddington luminosity for a  $10^7 M_{\odot}$  black hole (BH). Thus the Eddington or super-Eddington accretion rate is required in RX J1334.2+3759 provided that the mass of the central BH is  $\sim 10^7 M_{\odot}$ .

#### 4.3 Optical spectral characteristics

The optical spectrum of RX J1334.2+3759, shown in Fig. 6, appears to be typical of NLS1 galaxies. The FWHM velocity ( $\sim 2850$  km s<sup>-1</sup>) of the broad components of Balmer lines in the spectrum of RX J1334.2+3759 is similar to that found in the other NLS1 galaxies but is significantly lower than in the Seyfert 1 galaxies. For example, Grupe et al. (1999) found mean values of the broad components of H $\beta$  to be  $2790 \pm 160$  km s<sup>-1</sup> for a sample of NLS1s, and  $4210 \pm 360$  km s<sup>-1</sup> for a sample of Seyfert 1s.

Similarly, the ratio of fluxes of narrow and broad components of H $\alpha$  and H $\beta$ ,  $H_{\alpha_n}/H_{\alpha_b} = 1.8 \pm 0.46$ , and  $H_{\beta_n}/H_{\beta_b} = 1.26 \pm 0.37$ , for RX J1334.2+3759 are similar to those found in other NLS1 galaxies (Rodríguez-Ardila et al. 2000). This implies that the relative contribution of the broad components to the line flux is greatly reduced in RX J1334.2+3759 compared to that in the Seyfert 1 galaxies for which the ratio of narrow-to-broad component is around 0.1.

The narrow components of the permitted lines and the forbidden lines, such as [O III] $\lambda$ 5007, [N II] $\lambda$ 6583 etc., are thought to arise from the NLR of active galactic nuclei (AGNs). For RX J1334.2+3759, the flux ratio of the [O III] $\lambda$ 5007 line and the narrow component of H $\beta$ , [O III] $\lambda$ 5007/H $\beta_n$ , is  $0.30 \pm 0.06$  which is much smaller than the ratio of  $\sim 10$  found in Seyfert 2 galaxies. NLS1 galaxies, on the other hand, show values ranging from 0.5 to 5 for the [O III] $\lambda$ 5007/H $\beta_n$  ratio (see Rodríguez-Ardila et al. 2000). Thus, the NLR of RX J1334.2+3759 is different from the seven NLS1 galaxies in the sample of Rodríguez-Ardila et al. (2000).

RX J1334.2+3759 shows strong Fe II emission. The ratio of fluxes of Fe II and H $\beta$ , Fe II/H $\beta$ , is  $\approx 4.5$  for RX J1334.2+3759. This ratio is similar to that found in the other NLS1 galaxies (see Grupe et al. 1999).

In the following, we try to explain the observed flux ratios from the NLR and BLR of RX J1334.2+3759 and the other NLS1 galaxies in terms of density enhancements. In the same scenario, we also try to explain the well known anti-correlation between the slope of the soft X-ray continuum and the FWHM of the H $\beta$  line found in NLS1 galaxies. Eddington or super-Eddington accretion rates, thought to be responsible for the steep soft X-ray continua in NLS1s (see Pounds et al. 1995; Brandt & Boller 1998), may result in outflows. In the NLR of NLS1 galaxies, the flux ratio [O III] $\lambda$ 5007/H $\beta_n$  is smaller than the ratio found in the normal Seyfert galaxies. This smaller value can be produced by a smaller size of the NLR in NLS1 galaxies. Outflows can enhance the density of the BLR and extend its size outwards, thereby reducing the size of the NLR. In this scenario, the flux of the [O III] $\lambda$ 5007 line will be reduced while that of the narrow component of the permitted lines will not. Instead, the flux in the narrow components of the permitted lines is expected to increase because of an enhancement of the density. Thus, a smaller ratio of [O III] $\lambda$ 5007 and H $\beta_n$  can be produced in the NLR of NLS1 galaxies.

The FWHM of the broad component of the H $\beta$  line is significantly smaller in the NLS1 galaxies than those found in Seyfert 1 galaxies. It seems that in the NLS1 galaxies, appropriate physical conditions, where the maximum number of broad component H $\beta$  photons can be produced, are located at a larger radial distance from the nucleus than in the normal Seyfert 1 galaxies. This radial shift seems to be possible because of the outflows and a resulting enhancement in the density. The inner regions of the BLR in the NLS1 galaxies can be expected to be fully ionized in hydrogen as a result of the higher ionizing power of the steeper ionizing continua, and the temperature there can be higher than in the inner BLR of the Seyfert 1 galaxies. These kind of physical conditions in the inner BLR of the NLS1s will not, however, produce an appreciable number of H $\beta$  photons, while the outer regions of the BLR will have favourable physical conditions to generate a copious number of H $\beta$  photons. UV emission lines, which probe the inner BLR, are expected to be broader than the H $\beta$  line. Thus, an enhancement of the density as a result of outflows can explain (i) the lower width of H $\beta$  and H $\alpha$  in the NLS1s compared to Seyfert 1 galaxies, and (ii) comparable width of the permitted lines in the UV spectra of NLS1 galaxies compared to

Seyfert 1 galaxies. It should be noted that a relatively high density ( $\geq 10^{11} \text{ cm}^{-3}$ ) BLR has been inferred from the UV spectrum of I Zw 1 – a prototype NLS1 object (Laor et al. 1997b). There is also observational evidence for outflows in the NLS1 galaxies e.g. a weak UV absorption system with a line-of-sight outflow velocity of  $\sim 1870 \text{ km s}^{-1}$  has been detected from I Zw 1 (Laor et al. 1997b). Outflows in three other NLS1 galaxies, viz. Akn 564, WPVS007 and RX J0134.2 – 4258, have also been observed by the presence of UV absorption lines in their spectra (Goodrich 2000). In addition, Leighly et al. (1997) have found evidence for relativistic outflows in the ASCA spectra of three NLS1 galaxies. Higher accretion rates that would likely produce stronger outflows thus pushing the BLR further radially outward, thereby resulting in narrower Balmer lines in the NLS1 objects, also result in steeper soft X-ray continua. Thus, a variation in the higher accretion rate can result in the observed anti-correlation between the slope of the soft X-ray continua and the width of the  $H\beta$  line in the NLS1 objects.

Another advantage of the above picture is that the strong outflows can result in shocks which may be responsible for the Fe II emission observed in the NLS1 galaxies. Collin & Joly (2000) have shown that the standard photoionization models with any set of parameters cannot produce the observed strength of the Fe II emission in the NLS1 galaxies, and have suggested non-radiative heating, for instance, shock heating for the production of Fe II emission.

## 5 CONCLUSIONS

(i) RX J1334.2+3759, a newly discovered narrow-line quasar, is highly luminous in soft X-rays ( $L_X \sim 2.2 \times 10^{44} \text{ erg s}^{-1}$  in the energy band of 0.1–2.0 keV). Soft X-ray emission from RX J1334.2+3759 is very steep ( $\Gamma_X \sim 3.8$ ) and is highly variable. The most extreme variable event has  $\Delta L/\Delta t = (1.95 \pm 1.02) \times 10^{42} \text{ erg s}^{-2}$

(ii) The optical spectrum of RX J1334.2+3759 is typical of NLS1 galaxies. Decomposition of Balmer  $H\beta$  and  $H\alpha$  lines has revealed the presence of narrow (FWHM  $\sim 880 \text{ km s}^{-1}$ ) and broad components (FWHM  $\sim 2850 \text{ km s}^{-1}$ ) in them.

(iii) The ratio of the [O III] $\lambda 5007$  line flux and the flux in the narrow component of  $H\beta$  line is  $\sim 0.30$  which is very different from the value of  $\sim 10$  found in Seyfert 2 galaxies indicating that the NLR in RX J1334.2+3759 is different from the NLR in the normal Seyfert galaxies.

(iv) A possible explanation for the observed properties of the NLR and BLR of RX J1334.2+3759 and other NLS1 galaxies, as well as for the well known anti-correlation between soft X-ray slope and  $H\beta$  width found in them, has been suggested in terms of density enhancements resulting from outflows as a result of super Eddington accretion rates.

## ACKNOWLEDGMENTS

This research has made use of data obtained from the HEASARC, provided by NASAs Goddard Space Flight Center. We thank Todd Boroson and Richard Green for providing the Fe II template. IRAF is distributed by the National Optical Astronomy Observatories, which is operated by the Association of Universities, Inc. (AURA) under cooperative agreement with the National Science Foundation. The PROS software package was provided by the ROSAT Science data Center at Smithsonian Astrophysical Observatory. We thank an anonymous referee for comments and suggestions which improved the paper.

## REFERENCES

- Balucinska-Church M., McCammon D., 1992, *ApJ*, 400, 699  
 Boller Th., Trümper J., Molendi S., Fink H., Schaeidt S., Caulet A., Dennefeld M., 1993, *A&A*, 279, 53  
 Boller Th., Brandt W. N., Fink H., 1996, *A&A*, 305, 53  
 Boller Th., Brandt W. N., Fabian A. C., Fink H., 1997, *MNRAS*, 289, 393  
 Boroson T. A., Green R. F., 1992, *ApJS*, 80, 109  
 Brandt W. N., 1995, PhD thesis, Univ. Cambridge  
 Brandt W. N., Boller Th., 1998, *Astron. Nachr.*, 319, 163  
 Brandt W. N., Boller Th., 1999, in Gaskell C. M., Brandt W. N., Dietrich M., Dultzin-Hacyan D., Eracleous M., eds, *ASP Conf. Ser. Vol. 175, Structure and Kinematics of Quasar Broad Line Regions*. Astron. Soc. Pac., San Francisco, p. 265  
 Brandt W. N., Pounds K. A., Fink H., 1995, *MNRAS*, 273, L47  
 Brandt W. N., Boller Th., Fabian A. C., Ruzkowski M., 1999, *MNRAS*, 303, L53  
 Collin S., Joly M., 2000, *New Astronomy Reviews*, 44, 531  
 Dickey J. M., Lockman F. J., 1990, *ARA&A*, 28, 215  
 Fabian A. C., Rees M. J., 1979, in Barty W. A., Peterson L. E., eds, *X-ray Astronomy*. Pergamon Press, Oxford  
 Ferland G. J., Osterbrock D. E., 1986, *ApJ*, 300, 658  
 Forster K., Halpern J. P., 1996, *ApJ*, 468, 565  
 Goodrich R. W., 1989, *ApJ*, 342, 224  
 Goodrich R. W., 2000, *New Astronomy Reviews*, 44, 519  
 Grupe D., Beuermann K., Mannheim K., Bade N., Thomas H.-C., de Martino D., Schwobe A., 1995a, *A&A*, 299, L5  
 Grupe D., Beuermann K., Mannheim K., Thomas H.-C., Fink H. H., de Martino D., 1995b, *A&A*, 300, L21  
 Grupe D., Beuermann K., Thomas H. C., Mannheim K., Fink H. H., 1998, *A&A*, 330, 25  
 Grupe D., Beuermann K., Mannheim K., Thomas H.-C., 1999, *A&A*, 350, 805  
 Laor A., Fiore F., Elvis M., Wilkes B., McDowell J., 1997a, *ApJ*, 477, 93  
 Laor A., Jannuzi B. T., Green R. F., Boroson T., 1997b, *ApJ*, 489, 656  
 Leighly K. M., Mushotzky R. F., Nandra K., Forster K., 1997, *American Astronomical Society Meeting*, 191, 104.13  
 Lawrence A., Elvis M. S., Wilkes B. J., McHardy I., Brandt W. N., 1997, *MNRAS*, 285, 879  
 Mathur S., 2000, *MNRAS*, 314, L17  
 McHardy I. M. et al., 1998, *MNRAS*, 295, 641  
 Osterbrock D. E., Pogge R. W., 1985, *ApJ*, 297, 166  
 Osterbrock D. E., 1989, *Astrophysics of Gaseous Nebulae and Active Galactic Nuclei*. University Science Books, Mill Valley, California  
 Pfeiffermann E. et al., 1987, *Proc. SPIE Int. Soc. Opt. Eng.*, 733, 519  
 Phillips M. M., 1976, *ApJ*, 208, 37  
 Pounds K. A., Done C., Osborne J., 1995, *MNRAS*, 277, L5  
 Puchnarewicz E. M. et al., 1992, *MNRAS*, 256, 589  
 Remillard R. A., Grossan B., Bradt H. V., Ohashi T., Hayashida K., Makino F., Tanaka Y., 1991, *Nat*, 350, 589  
 Rodríguez-Ardila A., Binette L., Pastariza M. G., Donzelli C. J., 2000, *ApJ*, 538, 581  
 Rodríguez-Pascual P. M., Mas-Hesse J. M., Santos-Lleó M., 1997, *A&A*, 327, 72  
 Singh K. P., Barrett P., White N. E., Giommi P., Angelini L., 1995, *ApJ*, 455, 456  
 Thorne K. S., 1974, *ApJ*, 191, 507  
 Trümper J., 1983, *Adv. Space Res.*, 2, 241  
 Ulrich M. H., Comastri A., Komossa S., Crane P., 1999, *A&A*, 350, 816  
 Wandel A., 1997, *ApJ*, 490, 131  
 White N. E., Giommi P., Angelini L., 1994, *IAU Circ. No. 6100 (WGACAT)*

This paper has been typeset from a  $\text{\TeX}/\text{\LaTeX}$  file prepared by the author.